

Ocean surface waves in an ice-free Arctic Ocean

Jian-Guo Li¹

Received: 26 January 2016 / Accepted: 7 June 2016 / Published online: 18 June 2016
© Crown Copyright as represented by: UK Met Office 2016

Abstract The retreat of the Arctic ice edge implies that global ocean surface wave models have to be extended at high latitudes or even to cover the North Pole in the future. The obstacles for conventional latitude-longitude grid wave models to cover the whole Arctic are the polar problems associated with their Eulerian advection schemes, including the Courant-Friedrichs-Lewy (CFL) restriction on diminishing grid length towards the Pole, the singularity at the Pole and the invalid scalar assumption for vector components defined relative to the local east direction. A spherical multiple-cell (SMC) grid is designed to solve these problems. It relaxes the CFL restriction by merging the longitudinal cells towards the Poles. A round polar cell is used to remove the singularity of the differential equation at the Pole. A fixed reference direction is introduced to define vector components within a limited Arctic part in mitigation of the scalar assumption errors at high latitudes. The SMC grid has been implemented in the WAVEWATCH III model and validated with altimeter and buoy observations, except for the Arctic part, which could not be fully tested due to a lack of observations as the polar region is still covered by sea ice. Here, an idealised ice-free Arctic case is used to test the Arctic part and it is compared with a reference case with real ice coverage. The comparison indicates that swell wave energy will increase near the ice-free Arctic coastlines due to increased fetch. An expanded Arctic

part is used for comparisons of the Arctic part with available satellite measurements. It also provides a direct model comparison between the two reference systems in their overlapping zone.

Keywords Multi-resolution · Unstructured grid · Ocean surface wave · Arctic Ocean · Polar problems

1 Introduction

The Arctic sea ice coverage has shrunk at alarming speeds in recent summers, and climate scientists have predicted an essentially ice-free Arctic summer in the near future (Wang and Overland 2009). For instance, the Arctic ice edge retreated to as high as 86° N in the summers of 2007 and 2012. The disappearing Arctic summer sea ice has led to increased marine activities in the region, particularly cross-Arctic navigation along two well-known shipping routes, the North Sea Route and Northwest Passage. The foreseen requirement to forecast sea state in support of these marine operations in the Arctic has prompted ocean surface wave models to extend at high latitudes or even to include the North Pole. The major problem in extending a latitude-longitude (lat-lon) grid wave model at high latitudes is the diminishing longitude grid length towards the Pole, which exerts a severe restriction on time steps of finite difference schemes. Another problem is the increased curvature of the parallels at high latitudes, which erodes the scalar assumption of vector components defined relative to the local east direction, such as the meridian and zonal velocity components. Wave energy spectra in ocean surface wave models are discretised into directional components relative to the local east so they face the same scalar assumption problem as the velocity components at high latitudes.

Responsible Editor: Jose-Henrique Alves

This article is part of the Topical Collection on *the 14th International Workshop on Wave Hindcasting and Forecasting in Key West, Florida, USA, November 8–13, 2015*

✉ Jian-Guo Li
Jian-Guo.Li@metoffice.gov.uk

¹ Met Office, Fitzroy Road, Exeter EX1 3PB, UK

Among various grids developed to tackle the polar problems, the spherical multiple-cell (SMC) grid (Li 2011) is an efficient approach because it uses the same lat-lon grid cells and hence requires minimal changes to the lat-lon grid finite difference schemes. The SMC grid relaxes the Courant-Friedrichs-Lewy (CFL) restriction of the Eulerian advection time step by merging longitudinal cells towards the Poles as in the reduced grid (Rasch 1994). The merged cells also mitigate the restriction on diffusion time steps (Fourier number less than 1) as a diffusion term usually accompanies an advection scheme to smooth the so-called garden sprinkler effect of a discrete wave spectrum (Booij and Holthuijsen 1987). Round polar cells are introduced to remove the polar singularity of the spherical coordinate system. Vector component propagation errors caused by the scalar assumption at high latitudes are reduced by replacing the local east with a fixed reference direction to define the wave spectral components in the Arctic.

The SMC grid has been implemented into the WAVEWATCH III model (WW3, Tolman 1991; Tolman et al 2002; Tolman and WAVEWATCH III® Development Group 2014) and has been validated with classic numerical tests (Li 2011) and ocean surface wave observations (Li 2012). However, the Arctic part, in which a fixed reference direction is used to maintain the scalar assumption, cannot be fully tested against observations in the polar region as it is still covered by sea ice. This paper will use an idealised ice-free case to illustrate the SMC grid performance in the Arctic polar region. It also illustrates some potential wave environmental changes along the Arctic coastlines if the Arctic sea ice disappears. An expanded Arctic part is also used so that it covers some open sea surface and can then be compared with satellite observations. By comparing the expanded Arctic part with the original Arctic part, the two reference direction systems can then be compared directly within their overlapping area. Buoy wave spectral observations are also used for this validation study to ensure the consistency of the global model with the Arctic part.

2 SMC grid Arctic part

Numerical schemes for propagation of ocean surface waves on the SMC grid have been described in Li (2012). Here, the Arctic part-related materials will be briefly summarised for the convenience of describing the validation work. Most of the SMC grid propagation schemes are almost identical to those used on a conventional lat-lon grid because they share the same type of lat-lon mesh. So, in the polar region, a SMC grid faces the same singularity and directionality problems as a lat-lon grid. To remove the singularity at the North Pole, a polar cell centred at the North Pole is introduced in the SMC grid so that the singular differential equation is replaced with an integral one for the polar cell (Li 2011). To mitigate the degrading

of the scalar assumption of vector components due to the rapid changing local east direction at high latitudes, a fixed reference direction, the *map-east*, is used to define vector components above the given latitude, φ_A , in the Arctic. This polar region using the map-east reference direction is called the *Arctic part* of the SMC grid. For convenience, the rest of the SMC grid which uses the conventional local east reference direction will be referred to as the *global part*.

The map-east reference direction can be approximated by a rotated grid with its rotated pole at 180° E on the Equator. The angle from this approximated map-east to the local east at longitude λ and latitude φ is given by

$$\alpha = \text{sgn}(\cos\varphi\sin\lambda)\arccos\left[\frac{\cos\lambda\sin\varphi}{\sqrt{1-(\cos\lambda\cos\varphi)^2}}\right] \quad (1)$$

Propagation in the Arctic part still uses the same SMC grid as in the global part, but wave spectra in the Arctic part are redefined in reference to the map-east, instead of the local east. In addition, the polar cell does not have a local east direction so the map-east angle (Eq. (1)) is undefined at the North Pole. To define the polar cell wave spectrum in the map-east system, the map-east angle is chosen to be zero, which is equivalent to use a value with $\lambda = 0$ and φ slightly less than $\pi/2$ in Eq. (1). This missing local east at the North Pole does not affect the SMC grid propagation scheme as it is formulated in a C-grid style; that is, only the meridian velocity component at the edge of the polar cell is required (Li 2011).

Because the angle from the map-east to the local east varies with latitude and longitude, there are no fixed corresponding spectral components between the two systems. For this reason, wave spectra defined by local east cannot be mixed up with those defined from the map-east within the Arctic part. To separate these two parts in propagation schemes, the four rows just below the Arctic part are duplicated and attached to the Arctic part. The Arctic part is then treated as an isolated region with a virtual coastline at the edge of the outmost boundary cells. Similarly, the global part is treated as if it has a coastline at its north edge. To link up these two parts, the lower two boundary rows in the Arctic part are updated with wave spectra from the corresponding cells in the global part after they are rotated anticlockwise by α . For the global part, the top two rows are updated with wave spectra from the overlapping cells in the Arctic part after they are rotated clockwise by α . This overlapping boundary treatment is similar to the two-way nesting (Tolman 2008) except that different spectral reference directions are used in the two parts here.

Figure 1 shows the Arctic and UK regions of a multi-resolution (3–6–12–25 km) SMC grid, which is based on a lat-lon grid with a longitude increase of $\Delta\lambda = 360^\circ / 1024 = 0.3515625^\circ$ and a latitude increase of $\Delta\varphi = 180^\circ / 768 = 0.234375^\circ$. The cells are merged longitudinally at high

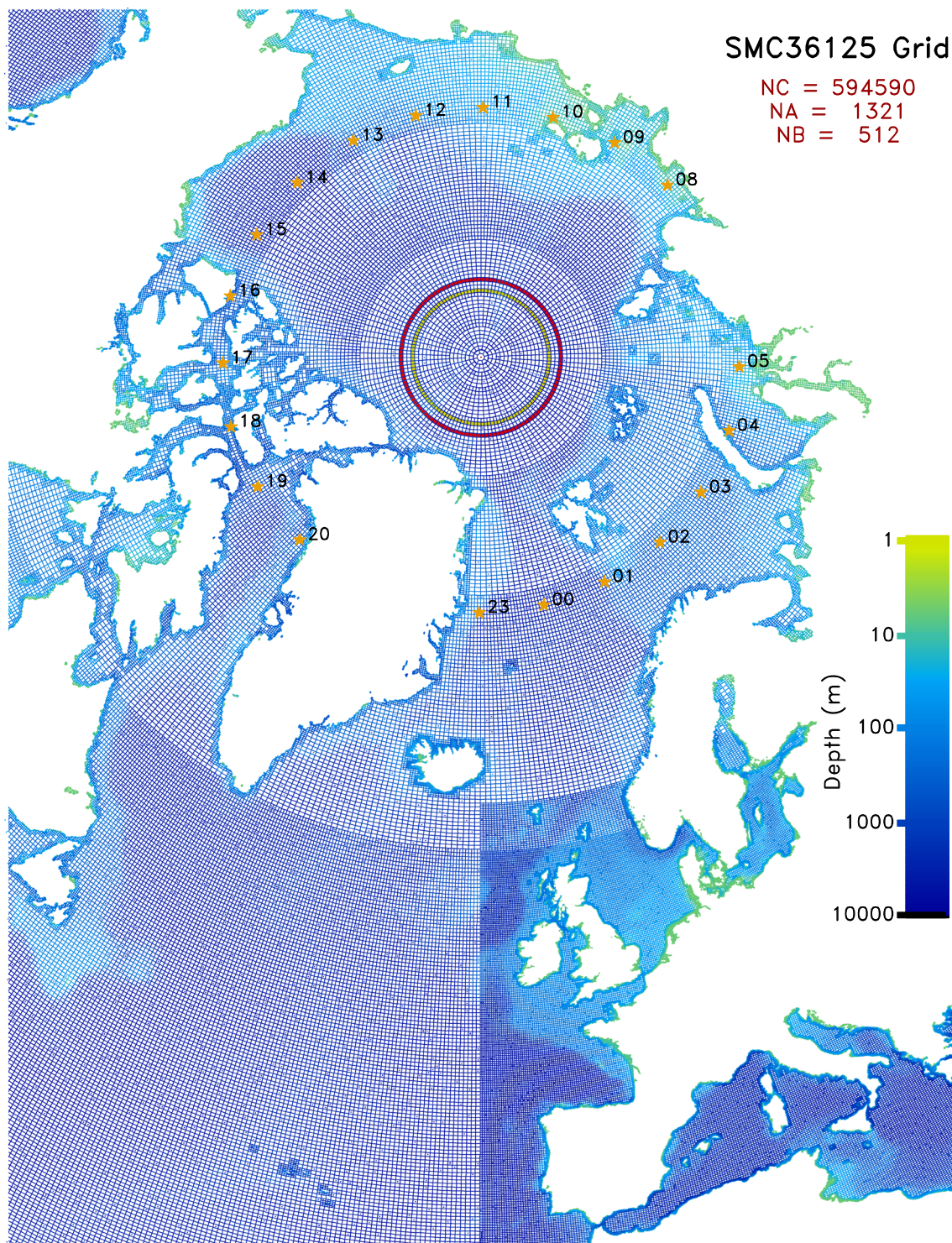


Fig. 1 The Arctic and UK regions of the SMC36125 grid

latitudes to relax the CFL restriction as described in (Li 2011). So, the base-resolution cells are about 25 km in physical distance. Near-coastline cells are refined by two more levels (12 and 6 km) except for the European region, where it uses three refined levels (12–6–3 km). The SMC grid refinement is similar to the quadtree mesh refinement (Popinet et al. 2010) and

does not need to keep all quadruplet cells, thanks to its unstructured feature. This makes the SMC grid quite useful for coastline refinement. The SMC36125 grid has been prepared for global and regional ocean surface wave forecasting in the Met Office (Li and Saulter 2014). The Arctic part (marked by the red circle in Fig. 1) is chosen above 85° N and the global

part ends at about 86° N (as indicated by the golden circle in Fig. 1). The Arctic part may be switched off if it is fully covered by sea ice. Because of the unstructured nature of the SMC grid, the Arctic cells are appended after the global part in a single-cell list for propagation. The two parts can then be conveniently separated by sub-loops so that it is convenient to switch off the Arctic part. The overlapping boundary rows are treated in the same way as other cells so the propagation is calculated together for both parts in a single loop. This allows maximum optimisation in parallel computations. Only the boundary cell update has to be treated as an extra calculation after each parallel propagation time step. The star points shown in Fig. 1 and marked by their time zone numbers (00–23) are selected for 2D spectral output. These 2D spectra will be used to study the wave spectral changes due to the disappearing Arctic sea ice.

Wind forcing for the Arctic part has to be converted into the map-east system as well. The conversion between the two systems uses the following transform:

$$\begin{pmatrix} u' \\ v' \end{pmatrix} = \begin{pmatrix} \cos\alpha & -\sin\alpha \\ \sin\alpha & \cos\alpha \end{pmatrix} \begin{pmatrix} u \\ v \end{pmatrix}, \quad \begin{pmatrix} u \\ v \end{pmatrix} = \begin{pmatrix} \cos\alpha & \sin\alpha \\ -\sin\alpha & \cos\alpha \end{pmatrix} \begin{pmatrix} u' \\ v' \end{pmatrix} \quad (2)$$

where u' and v' are the map-east velocity components, u and v are the corresponding local east velocity components and the cosine and sine of the map-east angle are given by

$$\cos\alpha = \frac{\cos\lambda\sin\varphi}{\sqrt{1-(\cos\lambda\cos\varphi)^2}}, \quad \sin\alpha = \frac{\sin\lambda}{\sqrt{1-(\cos\lambda\cos\varphi)^2}} \quad (3)$$

Propagation of each wave component is calculated together for both global and Arctic parts with the same propagation scheme except that the zonal and meridian group velocity components for the Arctic part are given by

$$u = c_g \cos(\theta' - \alpha), \quad v = c_g \sin(\theta' - \alpha) \quad (4)$$

where θ' is the spectral component angle from the map-east direction. Due to the fixed reference direction, the component propagation direction is also fixed in the Arctic part. The great circle turning (GCT) term (see Eq. 8 in Li 2012) has to be modified in the Arctic part to use the rotated grid latitude, which is close to zero in the Arctic part because the rotated equator passes the North Pole. If the Arctic part is kept small around the polar region (like above 85° N in the SMC36125 grid), this GCT term becomes negligible. The refraction term (see Eq. 7 in Li 2012) retains this formulation in the Arctic part, except that the gradients of water depth and current component along the wave direction have to be rotated to the map-east system. As the Arctic Ocean above 85° N is considered deep for wind waves, the refraction is also negligible in the small Arctic part.

A typical significant wave height (SWH) field from this model is shown in Fig. 2 on 6 September 2012 when the

Arctic sea ice coverage is close to the annual minimum. This figure is drawn cell by cell with a resolution of 250 colours within the SWH range from 0 to 22 m, and it demonstrates the smooth transfer between different resolution cells, such as the refined coastlines, the European region and the merged cells at high latitudes. The Arctic part is activated in this case because a tongue of open sea surface has extended into the Arctic part. Nevertheless, most of the Arctic part is still covered by sea ice, even at the minimum ice coverage time, so it is difficult to validate the fixed reference direction method with any observations within this Arctic part.

3 Expanded Arctic part

For validation of the map-east reference direction method with some satellite observations available in the Arctic, the Arctic part is expanded from the original 85° N to about 65° N (see Fig. 3a). As SMC grid cells have to be sorted by their sizes (in order to use sub-time steps for refined cells), the base-resolution cells are listed at the end. The Arctic part cells are currently appended at the end of the full cell list (for the convenience of switching it off) so they have to be at the base resolution. To ensure the expanded Arctic part (Axp) is still at the base resolution, the refinement near coastlines is suspended and a single-resolution (25 km) SMC grid is used for the Axp model. Another SMC grid at the same single resolution but with the original Arctic part (Arc) is also used for comparison purpose (see Fig. 4a). These single-resolution grids will be referred to as SMC25 Axp and Arc, respectively.

The test period was chosen to be August–September 2010 for available Envisat satellite ocean surface wave measurements. Satellite data points in the two months are overlaid on the Axp grid (Fig. 3a, orange dots), and they cover a fair area of the Axp Arctic part up to a maximum latitude of approximately 83° N. Two weeks were allowed for the models to spin up (from 1 August 2010) before comparing with satellite data. For comparison purposes, both models with the Arc and Axp configurations are run twice over the same period: one run with a normal ice fraction and another run ice-free. The ice-free runs are used to demonstrate how the map-east method handles the ocean surface wave propagation in the whole Arctic. The normal ice cases are used for comparison with satellite data. Besides, the two reference direction systems can be compared directly in the overlapping area between the global part of the Arc grid and the Arctic part of the Axp grid, i.e. between 65° N and 85° N, where the two different systems are used, respectively.

The source terms for this study use a locally tuned version of the WW3 ST4 scheme (Ardhuin et al. 2010). Major parameters different from the default ST4 ones include BETAMAX = 1.60, ZALP = 0.006 and Z0MAX = 0.002 in the name list SIN4 and SDSBR = 0.0009, SDSC2 = -2.6E-5

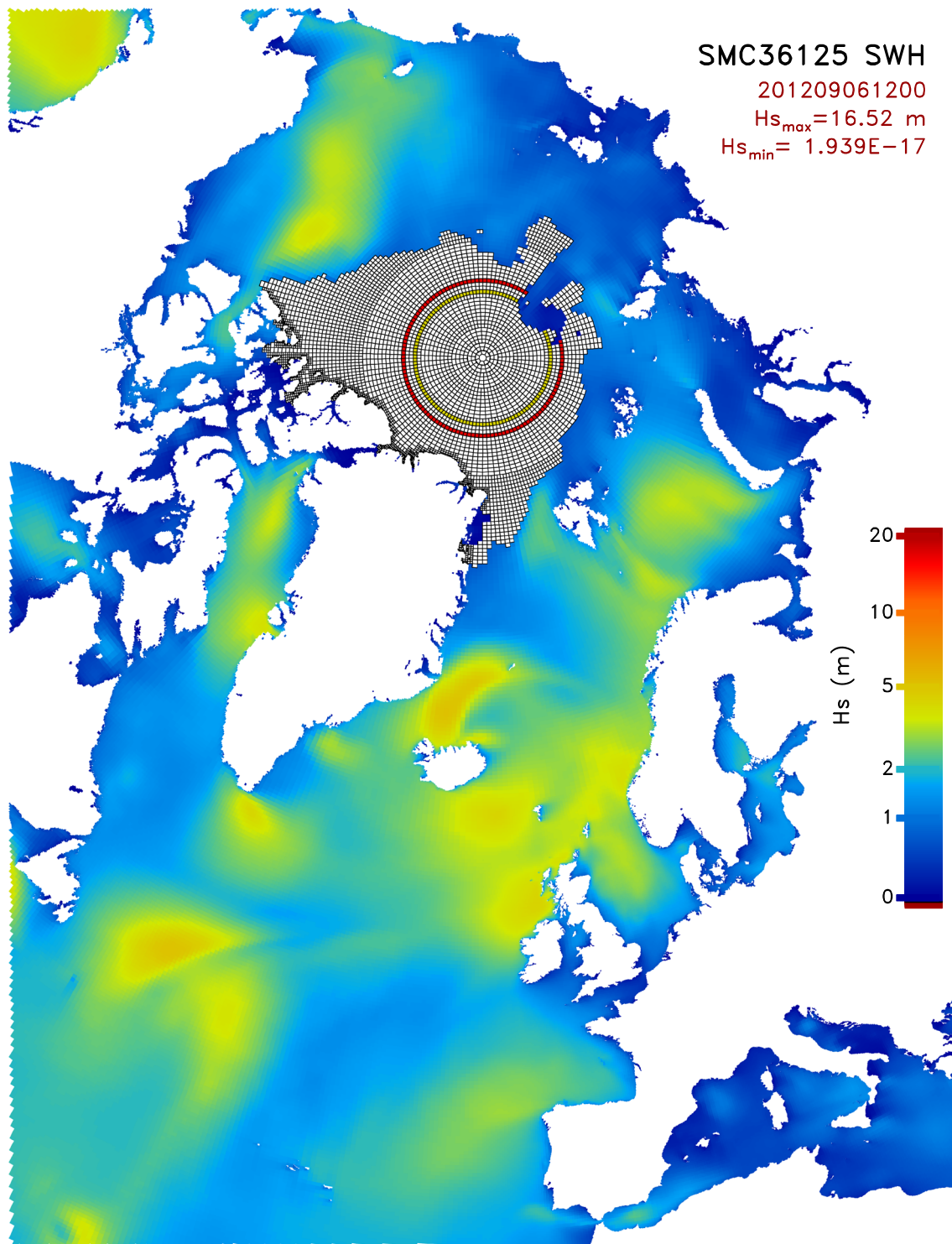


Fig. 2 SWH from the SMC36125 grid wave model on 6 September 2012

and $\text{FXFM3} = 2.5$ in the name list SDS4. The 25-km spatial resolution surface ice fraction (daily) and wind forcing (hourly) from the Met Office operational atmospheric model are used to drive the WW3 wave model. An upstream non-oscillatory second-order (UNO2) advection scheme (Li 2008), adapted from the Minmod scheme (Roe 1985), is combined

with a second-order diffusion term similar to that of Booij and Holthuijsen (1987) for wave transportation on the SMC grid. Partial sub-grid blocking similar to that of Tolman (2003) is used for the single-resolution SMC25 grids. Wave refraction and GCT terms are estimated with a rotation scheme, which is free from the CFL restriction but subject to the physical limit

Fig. 3 SMC25 Axp grid (a) and SWH fields for ice (b) and ice-free (c) cases. Available satellite data points are overlaid on the SMC25 Axp grid (a)

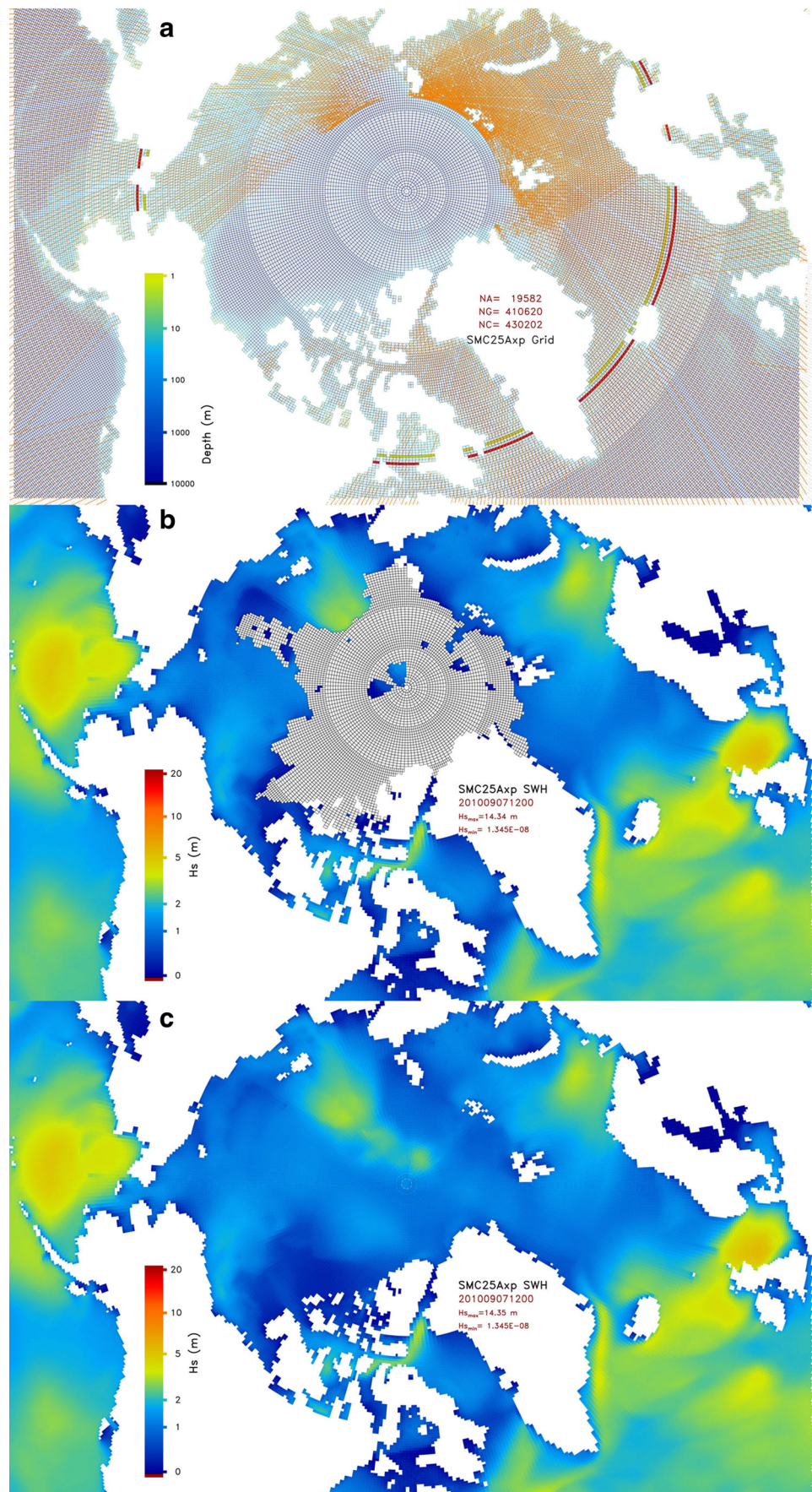
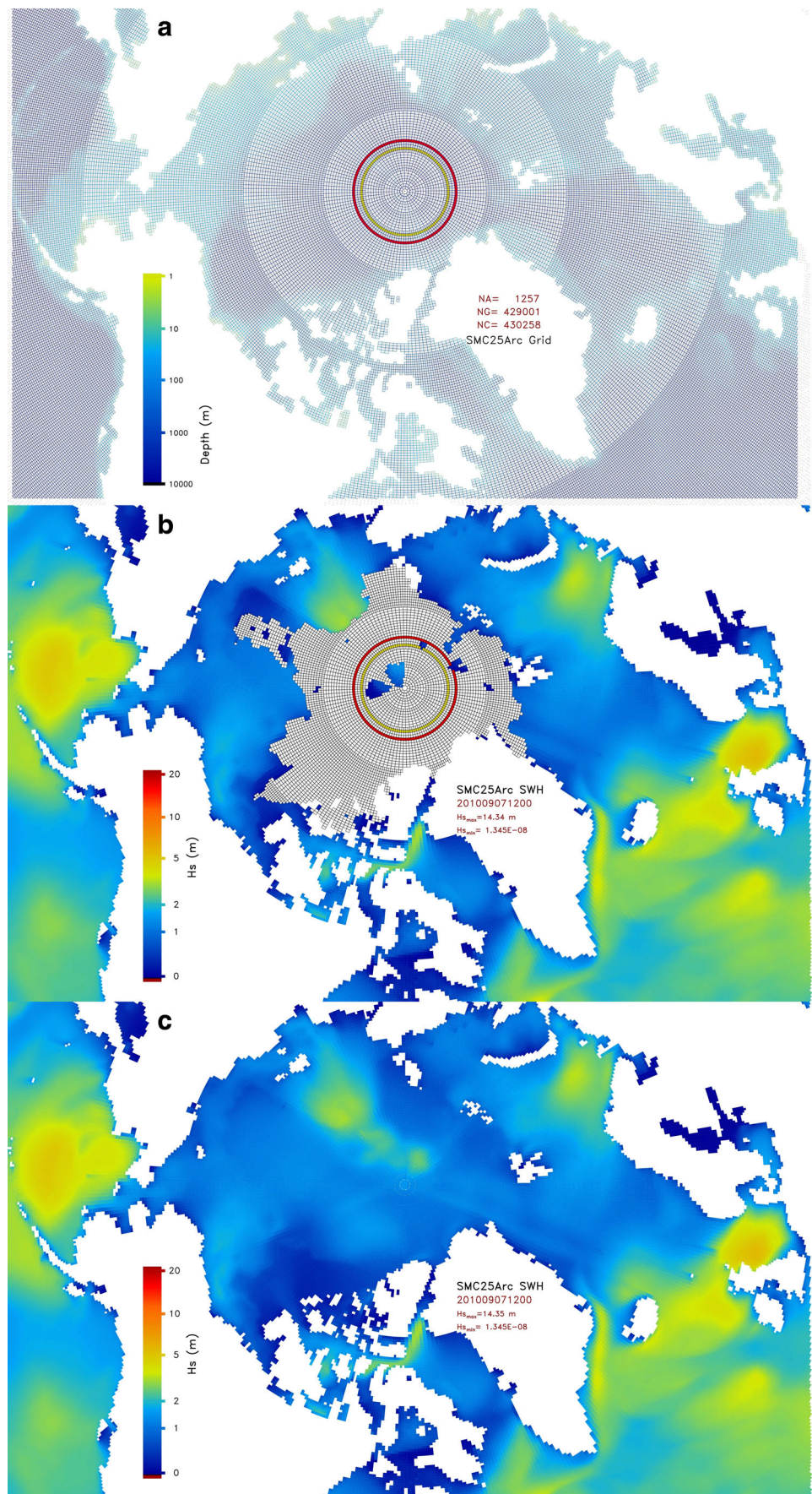


Fig. 4 The same as Fig. 3 but for the SMC25 Arc model with an Arctic part above 85° N, the same as used in the SMC36125 grid (see Fig. 1)



of maximum refraction angle up to the local gradient direction (Li 2012). The combined refraction and GCT term is switched off in the Arctic part in the WAVEWATCH III version 4.18 public release code because it is negligible within the original small Arctic part. For this study with the expanded Arctic part, the GCT and refraction terms are turned on in the Arctic part of both the Axp and Arc models to rule out any possible differences caused by these terms. These GCT and refraction updates for the SMC grid will be available in the next public release of WAVEWATCH III version 5 scheduled for mid 2016.

4 Validation of Arctic part

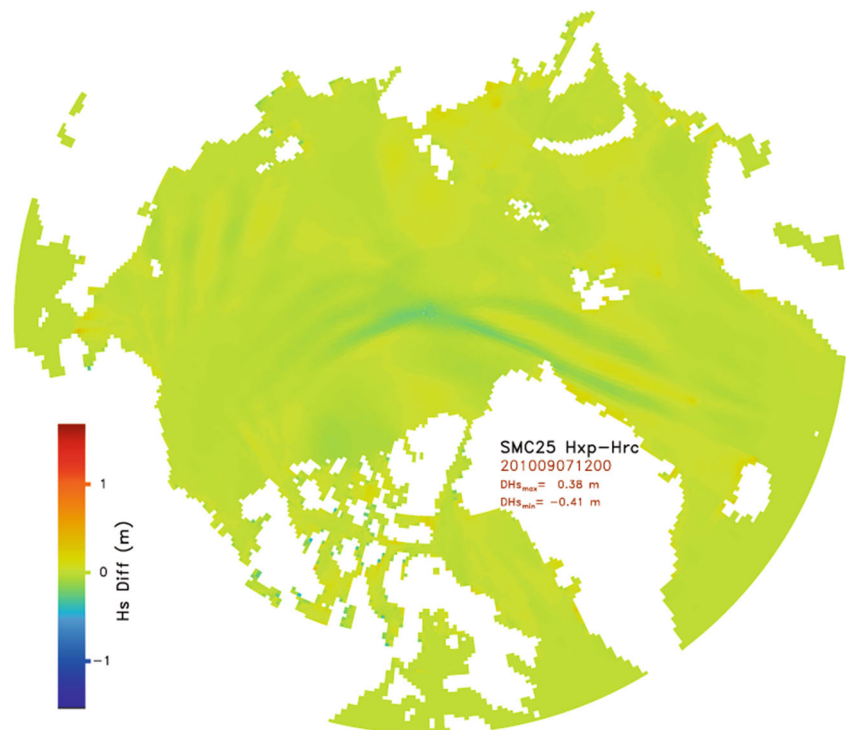
Figures 3b and 4b show the modelled SWH from the SMC25 Axp and Arc models with real sea ice on 7 September 2010, when the Arctic sea ice coverage is at approximately the annual minimum. The ice edge was mostly below 83° N that year, but some temporary polynyas were present above 83° N and even inside the original Arctic part (Fig. 4b). Figures 3c and 4c show the modelled SWH on the same date, but with the sea ice switched off. These ice-free runs allow the surface waves to travel freely over the whole Arctic Ocean, producing an ideal example for comparison of the two reference direction methods. The two runs generated almost identical SWH fields by a visual comparison of Figs. 3 and 4 for both ice and ice-free cases. The transition between the global and Arctic parts is continuous and smooth for both models, implying that both

the local east and map-east systems work almost equally well in the overlapping area between 65° N and 85° N.

The difference between the ice and ice-free cases in either the Axp (Fig. 3b, c) or the Arc model (Fig. 4b, c) is primarily caused by the extended fetch lengths in the ice-free case. For instance, the waves from the Atlantic may reach the Bering Strait across the ice-free Arctic Ocean. It could be envisaged that Arctic coastlines would expect more swell energy if the sea ice disappears in future summers. However, it has to be stressed that attributing this small difference in such a complicated model to a definite cause is risky because a lot of processes are related and difficult to isolate. For example, advection, refraction, and GCT schemes all have their inherent numerical diffusions, which depend on their speeds and directions (Li 2008). Any change in the transported field would result in changes in these numerical diffusions. These changes could not be easily pin-pointed or conveniently isolated from each other. Furthermore, source terms also depend on wave spectra and their effect may change as well if the wave spectra change.

Some subtle differences could be found between the two models in the expanded Arctic part as shown in Fig. 5 by the SWH difference between the ice-free cases of the two models (Figs. 3c and 4c). Figure 5 covers the area above 60° N so that both Arctic transition zones (around 65° N for the Axp model and 85° N for the Arc model) are included. The SWH from the two models is almost identical below 66° N, confirming that the transition between the Axp Arctic and global parts is smooth. The difference within the Axp Arctic part shows striped patterns parallel with swell paths, indicating that the

Fig. 5 SWH difference between the Axp and Arc models on 7 September 2010 at 1200 hours above 60° N



difference is caused by swells displaced by the two different systems. As the curvature-related errors in the local east system increase with latitude and become too large near the Pole, it is not a surprise that the two systems have some numerical differences in the overlapping region.

For a direct comparison of the two directional systems, Fig. 6 shows the scatter plots of SWH from the Axp and Arc models within the overlapping zone between 65° N and 85° N. The collocated model SWH values are at every 6 h during 1 month (September 2010) for all the open sea points between 65° N and 85° N, where the Arc model uses the local east reference direction while the Axp model uses the map-east one. Figure 6a shows the Axp-Arc SWH scatter plot for the runs with ice. There are 18,444 cells in the overlapping area, but only an average of about 14,248 entries for each of the 120 times are active or in open sea surface, resulting in a total of 1,709,747 pairs of SWH data for this plot. The two models are in a very good agreement with a nearly perfect correlation of 0.999 and a small root mean square (rms) difference of 0.036 m. It is not a surprise that the high wave or local wind sea is in better agreement than the low waves or swells because most of the differences are caused by slightly displaced swells. Nevertheless, the differences are very small in this overlapping zone and their effects are limited to swells. The probability density function (pdf) contour in Fig. 6 is defined with 80 bins for the 0–8 m range in each dimension, and the contour levels are set at 0.02, 0.1, 0.5 and 2.5 % to accommodate the steep slope of the density function. The collocated points are densely packed along the diagonal line, and there are only a few outlier points in the total selected data as the pdf contours indicate. Note that the scatter pattern is almost symmetrical to the diagonal line and major differences are in the low wave range, confirming that the difference is due to displacement of the swells between the two models.

Figure 6b shows the Axp-Arc SWH scatter plot for the ice-free case. In this case, all the 18,444 cells in the overlapping zone are active and the total number of paired entries increases to the full 2,213,280 pairs for the 120 selected times. The results also show a very good agreement (correlation 0.998) but a slightly increased rms difference from 0.036 to 0.047 m. This is reasonable because the curvature-induced errors increase when the open sea surface extends into high latitudes. Besides, increased fetch also allows swells to travel further and hence leads to a larger displacement error than in the ice case. This swell error increase is revealed by the bulging pdf contours at the low wave end in Fig. 6b. Nevertheless, the overall differences between the two models remain very small even in the fully opened Arctic Ocean. This indicates that the two reference direction systems perform almost equally well in the overlapping zone, so the small Arctic part within the polar region above 85° N can be considered good enough for solving the polar problem.

The above direct model comparison could not provide enough evidence about the model performance against real ocean surface waves. For a more objective assessment of the Arctic part performance, the models are validated with SWH observations from the radar altimeter (RA2) on board the European Space Agency (ESA) Envisat satellite. The satellite SWH data, about 7 km apart along satellite tracks, are collocated with interpolated model values to minimise the modification of the satellite data. This allows extra filters to be applied on the satellite data if required. For instance, spurious large satellite SWH values near coastlines pass through the ESA-recommended filters but can be filtered out by

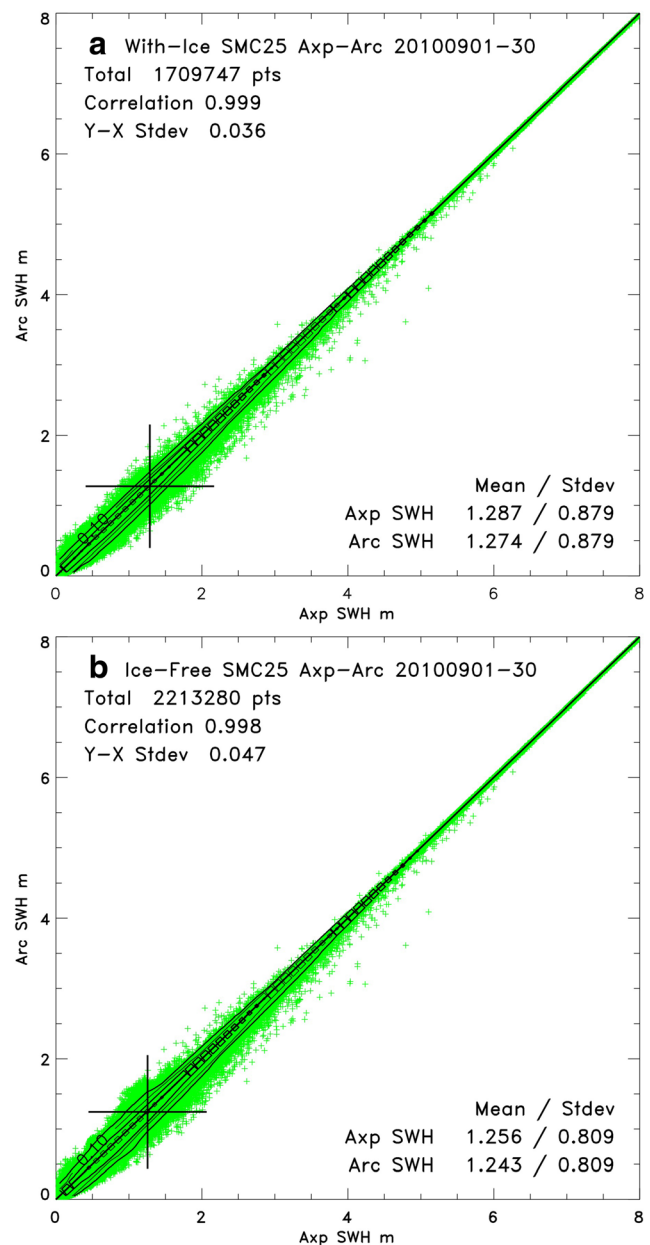


Fig. 6 Comparison of the Arc and Axp models' SWH between 65° N and 85° N for the ice (a) and ice-free (b) cases every 6 h in September 2010

comparing them to the interpolated model values (Li and Holt 2009; Li and Saulter 2012). Figure 7 compares the model and RA2 SWH along three satellite tracks, one crossing the Atlantic (Fig. 7a) and the other two passing the Pacific (Fig. 7b, c). They all span from the Southern Ocean to the

Arctic. The blue '+' symbols indicate the RA2 measurements. Some spurious large satellite values are shown close to coastlines or ice edges. These large outliers are difficult to remove with available data parameters so a simple filter, $SWH_{\text{satellite}} - SWH_{\text{model}} < 4 \text{ m}$, is introduced to mitigate their

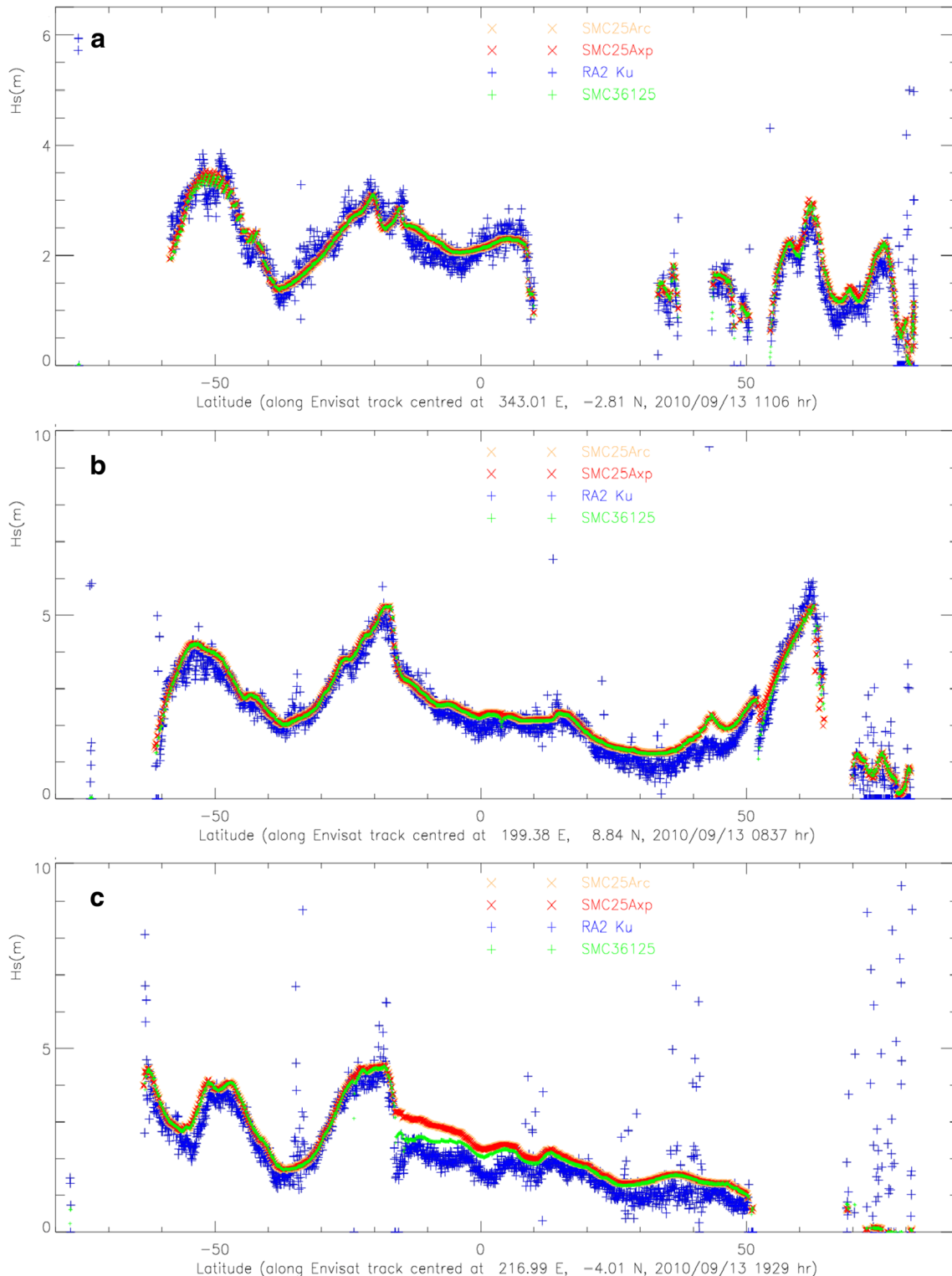


Fig. 7 a–c Comparison of SWH from the three models with RA2 data along the three Envisat satellite tracks on 13 September 2010

effect on the statistics. There are three model values comparing with each RA2 entry in Fig. 7. Apart from the SMC25 Arc (orange ×) and Axp (red ×) model values, the SMC36125 model SWH (green +) values are also shown. The Arc and Axp model values are almost overlapped on all the three tracks, including the Arctic sections. This confirms that the two reference direction methods are consistent in the Arctic in both the original Arc and expanded Axp cases. The SMC36125 model shows a slightly better agreement with the satellite data, particularly on the last Pacific track (Fig. 7c). This track (centred at 217° E and 4° S) passes over the French Polynesia region in the Pacific, where some small coral reefs are not resolved by the 25-km grid. The SMC36125 grid has 6-km refined resolution in this region and can resolve some of the small islands, hence a better blocking effect on swell than the SMC25 model.

The two panels in Fig. 8 show the model satellite scatter plots for the Arc (Fig. 8a) and Axp (Fig. 8b) models, respectively, over a 46-day period from 15 August to 30 September 2010 with ice. Only the satellite data in the expanded Arctic region (above 65° N) are used in Fig. 8, in order to highlight the statistical differences between the two systems. Note that there are no satellite observations above approximately 83° N so the comparison is effectively limited within the overlapping zone. As a result, Fig. 8 can be considered as an equivalent direct comparison of the two systems via the intermediate satellite data. Over 94,700 satellite entries are selected in this temporal and spatial slot. Despite of the use of all available filters, the scatter plots suggest that there are still many erroneous satellite values in the collocated data, as shown by the spread near the horizontal axis. The 4-m filter has effectively removed any satellite SWH values 4 m away from the diagonal line but does not have any effect on those values within the 4-m belt.

The differences between the Arc and Axp models can be derived by comparing Fig. 8a, b as they use the same satellite data. The difference is really small as both models produce similar correlations (0.738 and 0.737) and rms errors (0.652 and 0.655 m) against the same satellite measurement. Although the Arc model is slightly better than the Axp model in terms of correlation and rms errors, the Axp model mean (1.432 m) is closer to the satellite one (1.499) than that of the Arc model (1.417). So, it is hard to judge which method is better within the overlapping zone based on this comparison. The relatively low correlation (0.74) between the model SWH and satellite measurement may be attributed to the following two factors: (i) the SWH, in comparison with the global average, is relatively low within the polar region, and (ii) proportionally, more satellite data are likely to be contaminated by floating sea ice and coastal lands in the Arctic than in large ocean basins. Although the 4-m filter is applied, it is not sufficient to remove all the erroneous

altimeter data. Nevertheless, the influence is relatively small compared with the majority of satellite data, as indicated by the pdf contour lines in Fig. 8. The pdf contour levels are the same as used in Fig. 6. Furthermore, the satellite observation is used as an intermediary ‘ruler’ to measure the differences between the two models so small errors in the observation data are not very important as long as they are the same for both models.

The linear correlation between the satellite data and model SWH is improved if the comparison is extended to the whole globe as shown in Fig. 9. The increased correlation (from 0.74 to 0.95) is due to inclusion of some high waves, especially

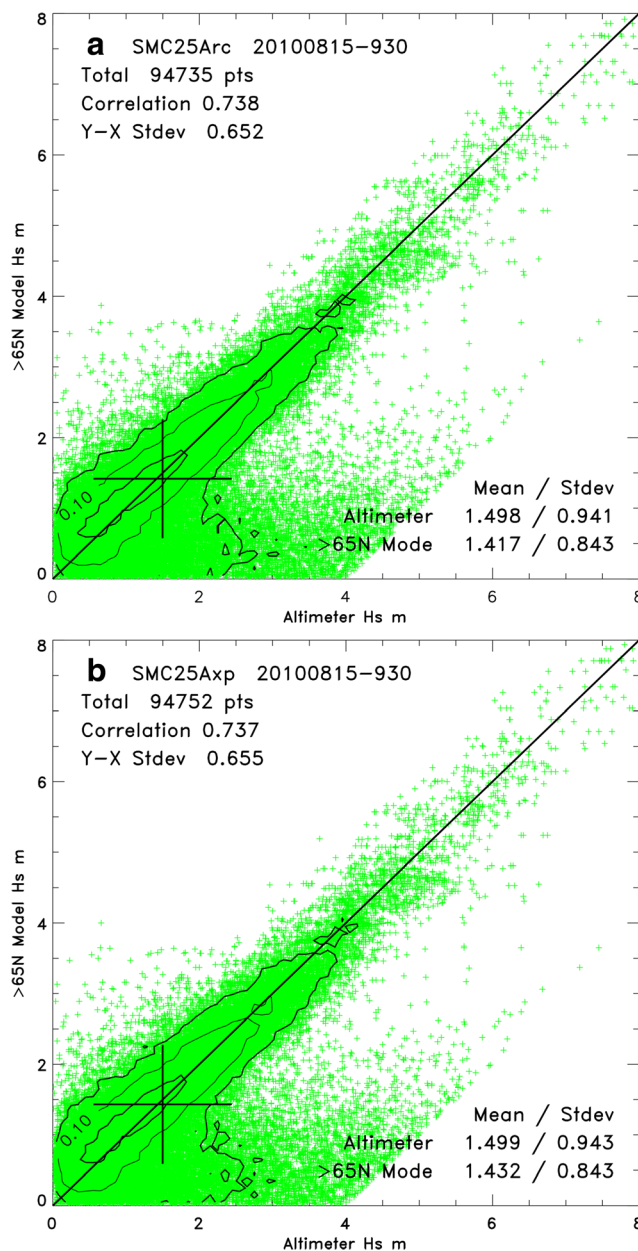


Fig. 8 Comparison of SMC25 Arc (a) and SMC25 Axp (b) models’ SWH with Envisat altimeter data from 15 August to 30 September 2010 in the polar region above 65° N

from the Southern Ocean. However, the larger match-up dataset masks the subtle differences between the two models. In fact, statistics for the Arc and Axp models are almost identical (the same correlation of 0.950, the same rms error of 0.465 m and the same RA2 mean of 2.555 m). The total numbers of selected RA2 data differ by 24 out of over 1 million entries, and the model means and standard deviations are only 0.001 m different. The small difference in the total number of selected data entries between the two global models reflects the subtle differences in the two models as some filters are model value dependent, such as the extra 4-m filter. Figure 9 confirms that the two Arctic parts show almost no difference on the global scale by the measure of satellite observations.

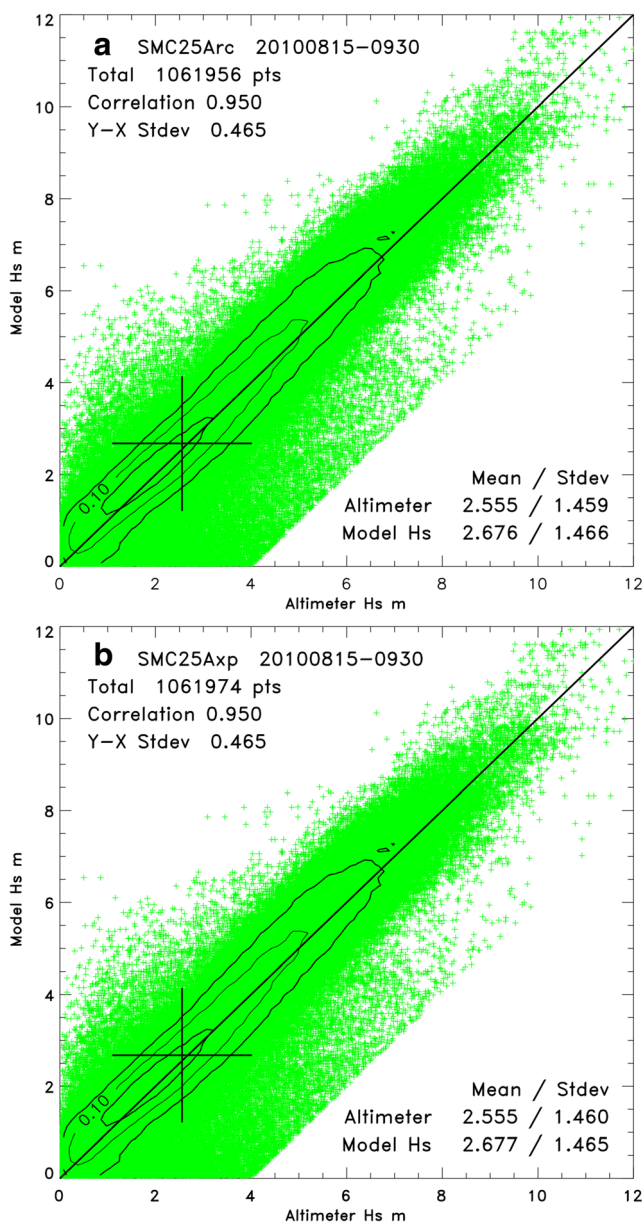


Fig. 9 The same as Fig. 8 but extended to full global comparison

5 Wave climate in ice-free Arctic

It is not difficult to predict that swell wave energy will increase along the Arctic coastlines or the two commercial shipping routes if the Arctic sea ice disappears. This is simply because the fetch increases dramatically in the Arctic Ocean if the polar ice block is removed, allowing waves to travel directly from the North Sea to the Bering Strait. To quantify the potential for wave climate change due to fetch alterations resulting from disappearing sea ice, the SMC36125 model is run for two cases, one with ice and another ice-free. The model run covers two months, August and September 2012, when the Arctic coastlines are ice-free in both cases. Full 2D wave spectra at the 20 selected points shown in Fig. 1 are saved from both runs, and they are used to reveal the spectral differences due to the sea ice change. Close examinations of wave spectra at these selected points have revealed that the sea ice change does not have much influence in sheltered areas, such as the 04 point at time zone 4 and 17–20 points along the Northwest Passage. The disappearing sea ice, however, has clearly increased the swell energy at exposed points. Figure 10a shows the SWH scatter plot between the ice and ice-free cases at the 15 exposed points (00–03, 05–16 and 23) every hour over 1 month (September 2012). The mean SWH increased from 1.39 m with ice (WIce) to 1.43 m in the ice-free case (NIce). The increase is mainly confined to low wave ranges as the scatter pattern reveals. For comparison, Fig. 10b shows the SWH scatter plot at the five sheltered points (04 and 17–20). The two cases generate almost identical wave heights in these points (a perfect correlation of 1.0 and a very small rms of 0.003 m), indicating that removing the Arctic sea ice does not affect these points.

For an approximate spectral analysis of the wave climate change due to disappearing Arctic sea ice, 4-bin sub-range wave height (SRWH) scatter plots are shown in Fig. 11. The SRWH is defined in analogue to the SWH but integrated over a limited frequency range (Li and Saulter 2012). The 4-bin margins are marked with the wave period (T) >16, 16–10, 10–5 and <5 s, respectively. The left four panels in Fig. 11 show the SRWH scatter plots at the 15 exposed points (the same as in Fig. 10a) between the ice and ice-free cases. They clearly reveal that the main increase of wave energy in the ice-free case is confined to moderate long waves (in the wave period range of 5–16 s). The local wind sea (bin $T < 5$ s) does not change much, nor do the very long waves (bin $T > 16$ s) because the fetch in the Arctic Ocean is limited to a maximum about 3000 km in the ice-free case. The increased swells in the ice-free case do not reach those five sheltered points, as indicated by the SRWH scatter plots on the right four panels in Fig. 11, where an almost perfect correlation (0.996–1.00) and a low rms difference (0.001–0.005) are found in all four sub-ranges. The SMC36125 model mean period output also confirms that the mean period along the exposed Arctic coastlines

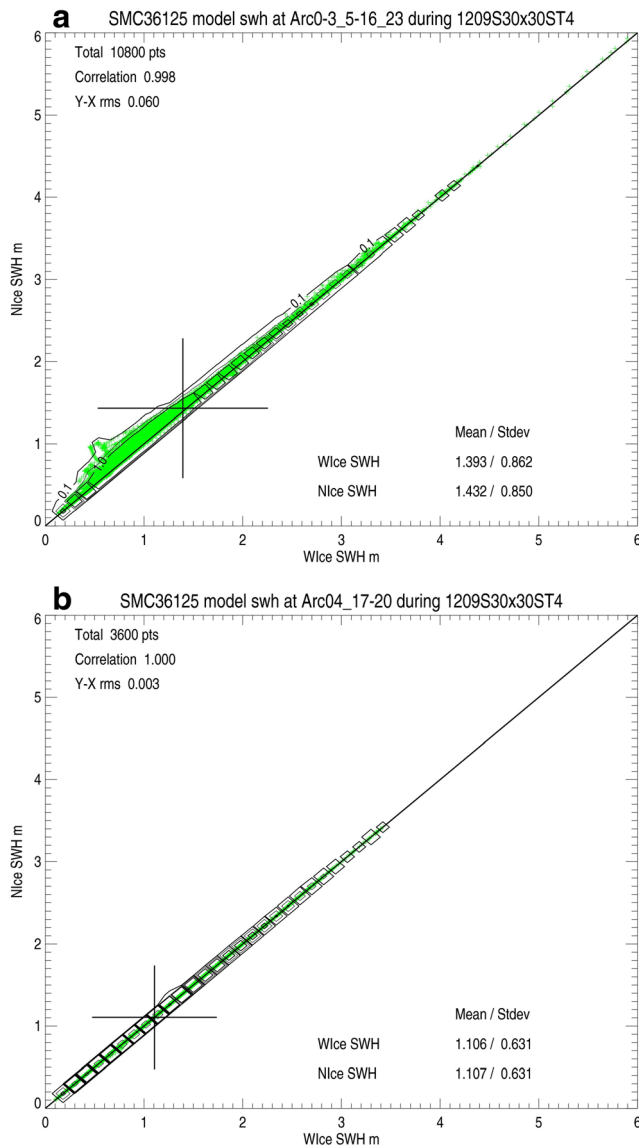


Fig. 10 Comparison of the SWH between ice and ice-free cases. **a** The exposed sites 00–03, 05–16 and 23. **b** The sheltered sites 04 and 17–20

increases from about 6 s in the ice case to about 8 s in the ice-free case. So, the disappearing Arctic sea ice will lead to an increase of wave height at Arctic coastlines, particularly along the North Sea Route, due to the arrival of some additional long-distance swells. It is worth pointing out that the same wind forcing is used in both the ice and ice-free cases. As the atmospheric wind forcing may be affected by the surface change, it would be ideal for this ice-free run to use a realistic ice-free wind. Nevertheless, the conclusion is unlikely to change significantly because the most important factor for the swell increase is the extended fetch.

Apart from possible sea surface rise caused by melting Arctic sea ice, the influence of Arctic sea ice change on ocean surface waves will primarily be restricted to the Arctic, as the ice-covered region is almost sheltered by the Arctic coastlines

from other oceans. To test that switching on the Arctic part in the SMC36125 model does indeed only affect its local regions, the SMC36125 model wave spectra are compared with the same spectral buoys as used in previous studies (Li 2012; Li and Saulter 2014), in which the Arctic part was switched off. These spectral buoys are all located outside the polar region so, as a result, switching on the Arctic part should not have any direct effect on them. Figure 12 compares the SMC36125 model ice run wave spectra with the spectral buoy observations over 4 months (September–December 2012). The SMC36125 model shows a slightly better agreement with the buoy spectra in Fig. 12 than the SMC6125 model ones in Li and Saulter (2014) (Fig. 4). The slight improvement of the SMC36125 model in buoy comparison cannot be attributed exclusively either to the active Arctic part or to the extra refined level (3 km around the European coastlines). The improvement is most likely due to an updated source term (ST4) used in the latest public release of WAVEWATCH III version 4.18 (Tolman and WAVEWATCH III® Development Group 2014). Figure 12 also shows the 4-bin SRWH scatter plots (bottom four panels) between the SMC36125 model and the spectral buoys. The agreement is satisfactory over the whole wave spectral range, although the model swell is slightly higher than the buoy measurement (first bin $T > 16$ s). The model wind sea is, however, slightly lower than the buoy value (fourth bin $T < 5$ s), and this partially cancels the model extra swell in the total wave energy budget. In fact, the total wave energy or SWH scatter plot (top panel in Fig. 12) yields a better agreement than the 4-bin individual plots. The model mean SWH (1.30 m) matches exactly with the buoy one. This example illustrates the usefulness of the spectral breakdown of wave energy into SRWH in comparison with the total wave energy or SWH. Actually, the local tuning of the source term is carried out with the aid of the 4-bin SRWH. The wind sea input rate is tuned by comparing the $T < 5$ s bin with buoy observations, and the swell dissipation is checked with the $T > 16$ s bin. Although this buoy comparison could not be used as a direct validation of the Arctic part, it confirms that the Arctic part is not affecting these buoy sites if compared with previous studies where the Arctic part was not activated.

6 Summary and conclusions

A SMC grid (Li 2011, 2012) has been installed in the WAVEWATCH III® model and is included in the last public released version 4.18 (Tolman and WAVEWATCH III® Development Group 2014). The SMC grid relaxes the CFL restriction at high latitudes by merging the longitudinal cells and removes the polar singularity by introducing a round polar cell. The unstructured nature of the SMC grid allows all land cells to be removed out of wave propagation and refined resolutions near coastlines or in any region of interest. The time

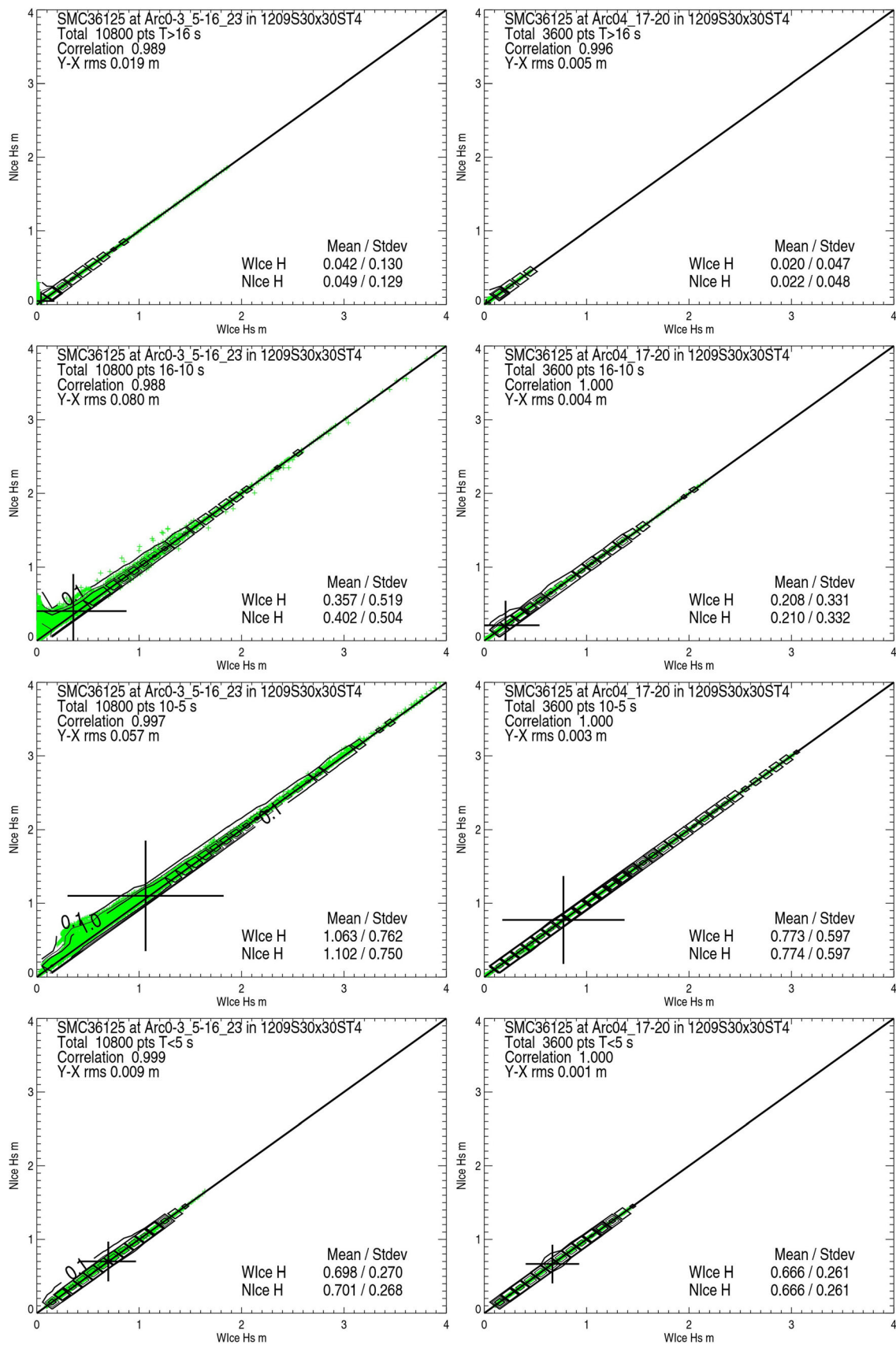
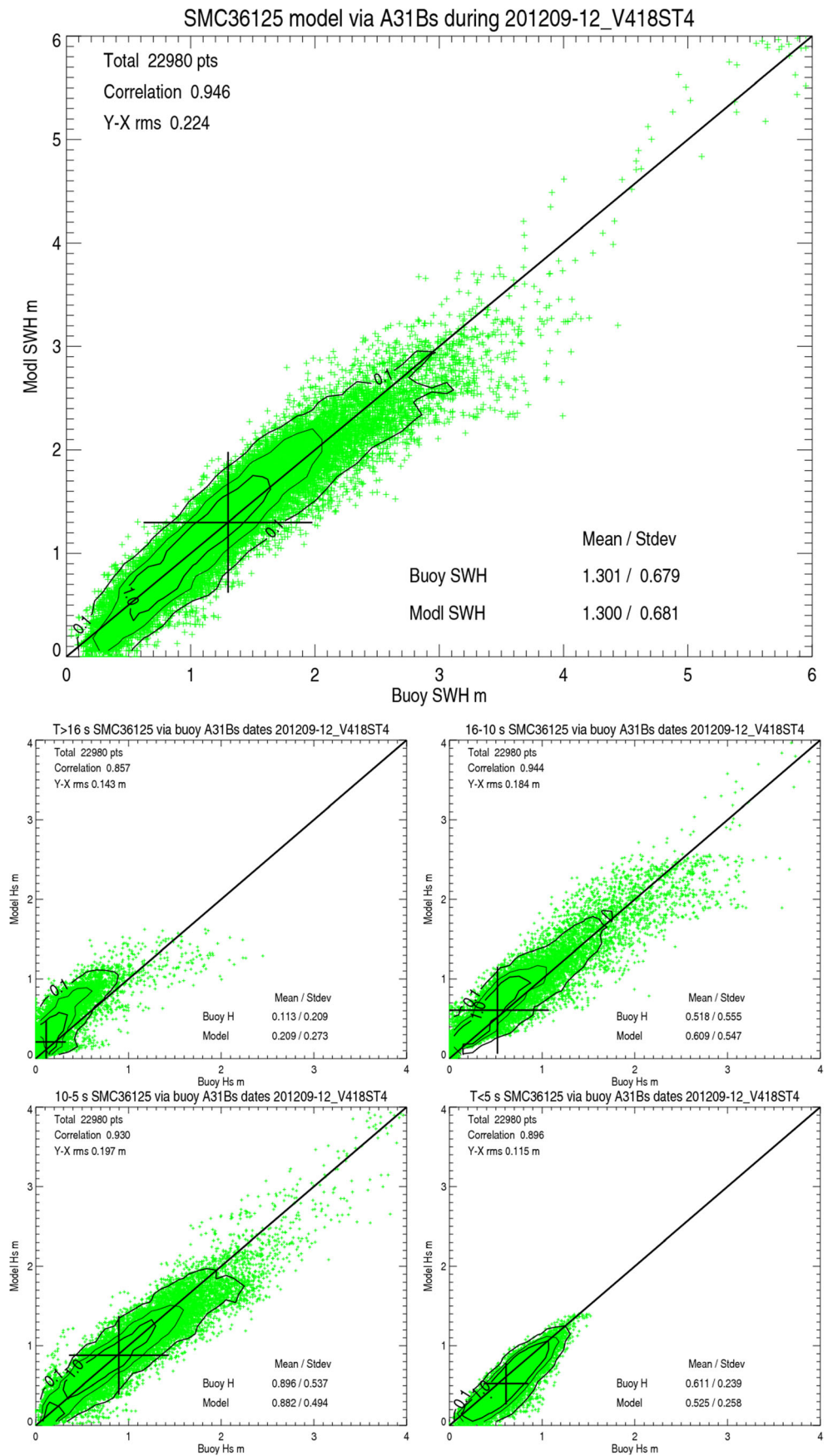


Fig. 11 Comparison of the SRWH between ice and ice-free cases. The *left column* is for the exposed sites 00–03, 05–16 and 23, and the *right column* is for the sheltered sites 04 and 17–20

Fig. 12 Comparison of the SMC36125 model SWH and 4-bin SRWH with buoy observations over 4 months from September to December 2012



step relaxation at high latitudes and the use of sub-time steps for refined resolutions result in a substantial computing cost reduction in comparison with a conventional latitude-longitude grid model.

A simple solution to the polar problem, caused by the rapid change of local east directions over merged cells or on a reduced grid, has also been applied. A map-east reference direction is introduced to define vector wave spectral components in a small polar region (Arctic part), so that the scalar assumption can be maintained at high latitudes. This method makes it possible to expand global wave models to cover the whole Arctic in response to sea ice retreat in future summers. The map-east method is demonstrated with ocean surface wave modelling in an ice-free Arctic and is directly validated with available satellite observations in an expanded configuration.

Results of model-model comparisons and validation against satellite data indicate that the map-east method works in the polar region and is consistent with the conventional local east method between 65° N and 85° N. The transition between parts of the grid using the two different direction systems is seamless and smooth. The correlation of model and satellite SWH in the Arctic region was found to be generally lower than that for the full global comparison, but this is primarily due to the quality of satellite observations, rather than the wave model grid scheme. Comparisons of model wave spectra, via the 4-bin sub-range wave height SRWH, between the ice and ice-free cases indicate that the disappearing Arctic sea ice will lead to an increase of wave height at Arctic coastlines, particularly along the North Sea Route, due to the arrival of some extra long-distance swell energy. This wave climate change caused by the retreating Arctic sea ice will be limited within the Arctic due to its coastline barriers.

The SMC36125 model is also compared with the same spectral buoy observations as used in Li and Saulter (2014), and the results show that the global model is consistent when the Arctic part is included. This study also confirms that the multi-resolution SMC36125 grid is better than the single-resolution ones in the full range of the ocean surface waves due to resolving small islands with refined resolutions.

Acknowledgments The author is grateful to Dr. Andrew Saulter (Met Office) and the two anonymous reviewers for their constructive suggestions to improve this manuscript.

References

- Ardhuin F, Rogers E, Babanin A, Filipot JF, Magne R, Roland A, Van der Westhuysen A, Queffelec P, Lefevre JM, Aouf L, Collard F (2010) Semiempirical dissipation source functions for ocean waves. Part I: definition, calibration and validation. *J Phys Oceanogr* 40:1917–1941
- Booij N, Holthuijsen LH (1987) Propagation of ocean waves in discrete spectral wave models. *J Comput Phys* 68:307–326
- Li JG (2008) Upstream non-oscillatory advection schemes. *Mon Weather Rev* 136:4709–4729
- Li JG (2011) Global transport on a spherical multiple-cell grid. *Mon Weather Rev* 139:1536–1555
- Li JG (2012) Propagation of ocean surface waves on a spherical multiple-cell grid. *J Comput Phys* 231:8262–8277
- Li JG, Holt M (2009) Comparison of Envisat ASAR ocean wave spectra with buoys and altimeter data via a wave model. *J Atmos Oceanic Tech* 26:593–614
- Li JG, Saulter A (2012) Assessment of the updated Envisat ASAR ocean surface wave spectra with buoy and altimeter data. *Remote Sens Environ* 126:72–83
- Li JG, Saulter A (2014) Unified global and regional wave model on a multi-resolution grid. *Ocean Dyn* 64:1657–1670
- Popinet S, Gorman RM, Rickard GJ, Tolman HL (2010) A quadtree-adaptive spectral wave model. *Ocean Model* 34:36–49
- Rasch PJ (1994) Conservative shape-preserving two-dimensional transport on a spherical reduced grid. *Mon Weather Rev* 122:1337–1350
- Roe PL (1985) Large-scale computations in fluid mechanics. In: Engquist E, Osher S, Somerville RJC (eds) *Lectures in applied mathematics*, vol 22., pp 163–193
- Tolman HL (1991) A third-generation model for wind waves on slowly varying unsteady and inhomogeneous depths and currents. *J Phys Oceanogr* 21:782–792
- Tolman HL (2003) Treatment of unresolved islands and ice in wind wave models. *Ocean Model* 5:219–231
- Tolman HL (2008) A mosaic approach to wind wave modeling. *Ocean Model* 25:35–47
- Tolman HL, WAVEWATCH III® Development Group (2014) User manual and system documentation of WAVEWATCH III® V4.18. Techn Note 316, NOAA/NCEP, 311 pp
- Tolman HL, Balasubramanian B, Burroughs LD, Chalikov DV, Chao YY, Chen HS, Gerald VM (2002) Development and implementation of wind-generated ocean surface wave models at NCEP. *Weather Forecast* 17:311–333
- Wang M, Overland JE (2009) A sea ice free summer Arctic within 30 years? *Geophys Res Lett* 36:L07502, 5 pp